ACS Catalysis

Research Article

Cite This: ACS Catal. 2019, 9, 10951−10962

pubs.acs.org/acscatalysis

Impact of Specific Interactions Among Reactive Surface Intermediates and Confined Water on Epoxidation Catalysis and Adsorption in Lewis Acid Zeolites

Daniel T. Bregante and David W. Flaherty*

Department of Chemical and Biomolecular Engineering, University of Illinois at Urbana−Champaign, Urbana, Illinois 61801, United States

Supporting Information

ABSTRACT: Molecular interactions at solid−liquid interfaces greatly influence the stability of surface intermediates central to adsorption and catalysis. These complex interactions include the reorganization of solvent molecules near active sites to accommodate the formation of reactive surface intermediates. The consequences of these interactions and how they depend on the chemical functionality of the extended surface within pores have not been demonstrated in ways that permit the rational use of excess thermodynamic properties in the design of catalytic sites. Here, we show that adsorption enthalpies and entropies for 1,2-epoxyoctane ($C_8H_{16}O$) increase by 19 kJ mol^{-1} and 75 J mol^{-1} K^{-1}, respectively, when the density of silanol nests decrease from ∼5 to 0 $(unit\ cell)^{-1}$ within Ti-substituted zeolite BEA (Ti-BEA) in the presence of trace H_2O. In contrast, these properties are indistinguishable across all Ti-BEA samples under anhydrous conditions, which suggests that H_2O proximate to Ti adsorption sites interacts with bound $C_8H_{16}O$. In situ infrared spectra of hydrophilic Ti-BEA show that coordination of $C_8H_{16}O$ to framework Ti-sites reduces the extent of hydrogen bonding with and among H_2O molecules, which is reflected by changes in the frequencies of O−H stretching modes and molecular librations. Adsorption of $C_8H_{16}O$ into hydrophobic Ti-BEA, however, does not cause detectable changes in the vibrational spectra of nearby H_2O. The combination of these results, along with values of activation enthalpies and entropies for epoxidation reactions in the same materials, show that the disruption of hydrogen-bonded H_2O near Ti-atoms introduce excess free energies of adsorption that can be manipulated by controlling the number of solid- and liquid-phase hydrogen bond donors and acceptors at interfaces. These findings reveal the complex role of surface moieties on epoxidation reactions in Ti-silicates, show how silanol groups may impact other liquid-phase reactions within zeolites, and provide a basis to understand the manner by which surface chemistry impacts the structure of surrounding solvent molecules.

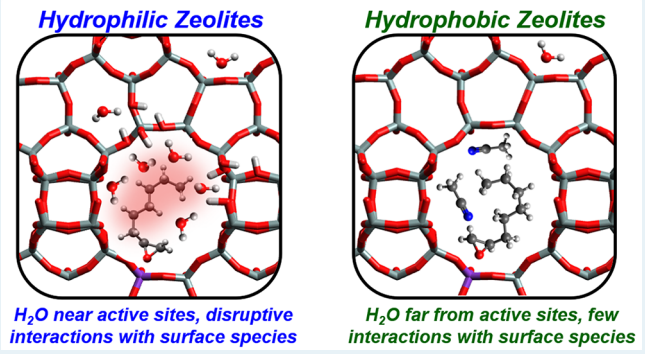

KEYWORDS: *hydrophobic zeolites, silanol nests, solvent effects, excess free energies, solid−liquid interfaces, calorimetry, solvent structure*

1. INTRODUCTION

Zeolite and zeotype materials are attractive scaffolds for catalytic and separation processes, due to their ability to discriminate among molecules by size exclusion and shape selectivity.[1,2] When zeolite pores are largely vacant, van der Waals interactions with surfaces contribute to the stability of adsorbates and reactive intermediates that bind to active sites. The level of complexity increases further when pores contain liquid-like densities of molecules that can assemble into structures governed by specific interactions among these molecules and with surfaces. Adsorption and reaction at active sites surrounded by solvation shells requires that these structures change to accommodate the surface species that form, which introduces excess free energy differences to adsorption, reaction, and activation processes.[3−7]

Hydrogen-bonding interactions between entrained solvent molecules (e.g., R−OH; R = H, alkyl), adsorbates, and surfaces within microporous materials affect uptake, intrapore diffusion, and surface reactions and have been implicated in studies that focus on the adsorption of alcohols and water in microporous solids,[8−15] the enhancement of water transport via highly structured hydrogen-bonded networks within carbon nanotubes,[16−20] the formation and stabilization of hydronium ions within zeolites,[21,22] and liquid-phase oxidations within micro- and meso-porous silicates.[4,23−32] For example, silicalite-1 synthesized in OH^- media (MFI−OH) adsorbs significantly

Received: August 5, 2019
Revised: September 26, 2019
Published: October 25, 2019

DOI: 10.1021/acscatal.9b03323
ACS Catal. 2019, 9, 10951−10962

Scheme 1. Changes in Free Energy Due to (a and b) Formation of the C_8H_{16} Epoxidation Transition State and (c and d) Adsorption of $C_8H_{16}O$ over (a and c) Hydrophobic and (b and d) Hydrophilic Ti-BEA to Show Exaggerated Changes in Solvent Structure[a]

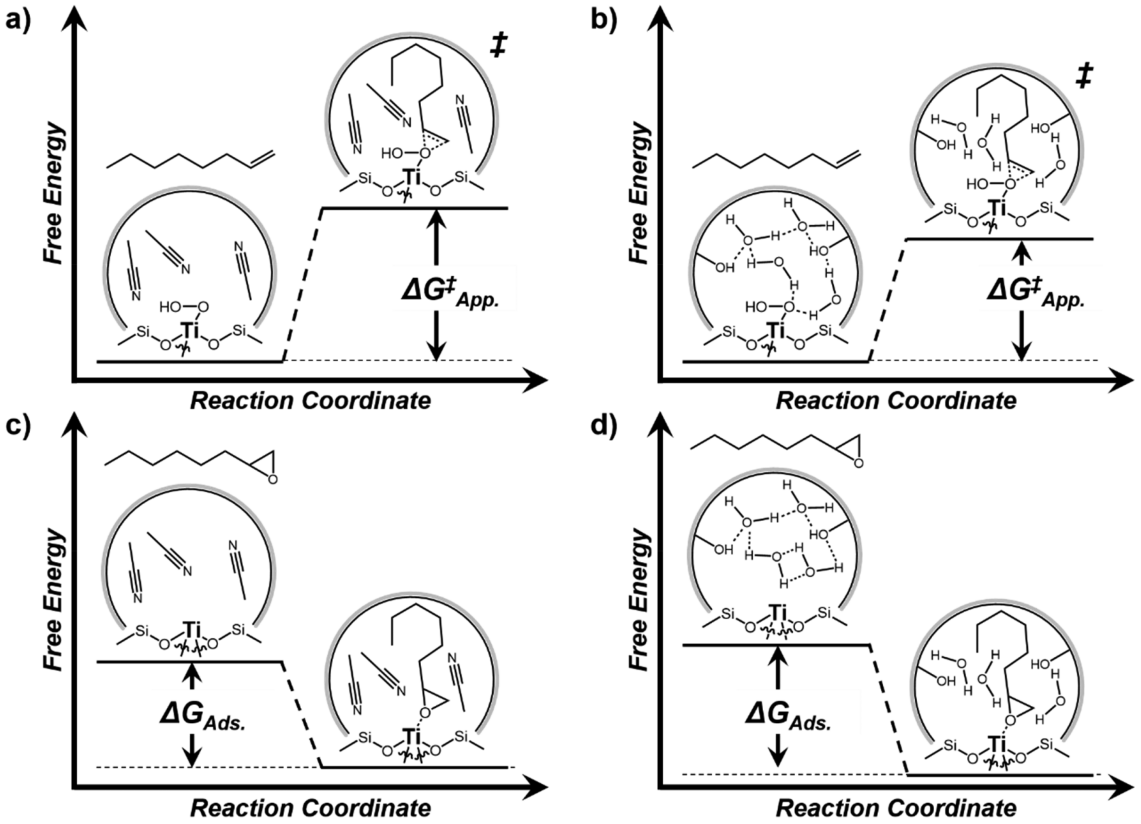

[a]These thermochemical sequences for C_8H_{16} epoxidation and $C_8H_{16}O$ adsorption have Ti-OOH and solvent-covered Ti active sites with fluid-phase C_8H_{16} and $C_8H_{16}O$ as the reference states, respectively. Dashed lines in the reference states provide a visual representation of the hydrogen-bonding network of H_2O within hydrophilic Ti-BEA.

more water below and near the saturation pressure ($P/P_0 \approx 0.95$) than silicalite-1 crystallized in F^- media, because the greater density of internal silanol (SiOH) defects in MFI−OH assist in stabilizing hydrogen-bonded H_2O clusters.[8,33−35] For decades hydrophobic Ti-silicates have been reported to be more productive catalysts for epoxidations, in comparison to analogous hydrophilic structures, which was ascribed to enrichment of alkene reactants near active sites or to increased rates of alkene diffusion in different studies.[28,30,36−42] Recent results from our group[4] and others[28,39,41] show, however, that the presence of internal SiOH groups increases rates and selectivities for alkene epoxidations when water is present in the solvent. These observations seem inconsistent with previous hypotheses for the mechanisms by which SiOH affect epoxidation reactions and require alternative explanations, and specifically, ones that address the stabilities of relevant transition state structures.

The stability of transition states for epoxidations, but also numerous other liquid-phase reactions, depend on chemical interactions between these structures and the surrounding solvent molecules, and these interactions impact catalytic rates and selectivities as a result.[3,5,43] Dumesic and co-workers used a combination of rate measurements and ab initio molecular dynamics to evince linear free energy relationships that quantitatively describe changes in the extent of solvation (i.e., solvation shells of H_2O and cosolvents) between the initial and transition states for acid-catalyzed dehydration reactions of sugars and alcohols, which can lead to a nearly 400-fold increase in rates.[44−46] These results demonstrate the manner by which specific interactions with H_2O confer stability to activated complexes and facilitate homogeneous reactions, but we are not aware of demonstrations for similar phenomena at solid−liquid interfaces. As such, the community lacks molecular descriptions and quantitative relationships that describe the interaction among confined solvent molecules (e.g., H_2O), reactive species at active sites, and the extended surface of solid catalysts that can demonstrate how these interactions impact adsorption and catalysis.[3,4,25−27,31,47]

Rates and selectivities for 1-octene (C_8H_{16}) epoxidation are 100-fold greater in Ti-BEA materials that contain ∼5 silanol nests ($(SiOH)_4$) (unit cell)$^{-1}$ in comparison to hydrophobic, defect-free Ti-BEA.[4] These findings contradict earlier reports for alkene epoxidation in Ti-silicates (vide infra) that emphasized the need to eliminate SiOH defects to concentrate alkene reactants near active sites or to alleviate diffusional constraints. These differences in rates and selectivities were attributed to excess enthalpies ($H^{\ddagger,\varepsilon}$) and entropies ($S^{\ddagger,\varepsilon}$) of C_8H_{16} epoxidation transition states (Scheme 1a and b) caused by interactions of the aliphatic octyl chain with proximate H_2O structures stabilized at nearby $(SiOH)_4$ groups. The putative cause of these excess quantities is the need for solvent structures to reorganize to accommodate the formation of reactive surface intermediates as the reaction progresses throughout the catalytic cycle. The differences in catalytic

DOI: 10.1021/acscatal.9b03323
ACS Catal. 2019, 9, 10951−10962

behavior between defective and defect-free Ti-BEA materials suggests that interactions between solvent molecules, reactive intermediates, and the catalyst surface have consequences for catalysis. These proposals result largely from the analysis and interpretation of kinetic measurements, and therefore, direct observations for changes in the structure of the solvent and quantitative measures of the impact on elementary steps relevant for catalysis are needed to gain deeper understanding of the role of these solvent-mediated processes for reactions within microporous materials.

Here, we report calorimetric and spectroscopic evidence that differences in the thermodynamics of 1,2-epoxyoctane ($C_8H_{16}O$) adsorption in Ti-BEA reflect changes in the solvent structure about active sites and that these changes can be controlled by intentionally incorporating SiOH defects near Ti atoms (Scheme 1c and d). Results from isothermal titration calorimetry (ITC) show that adsorption enthalpies and entropies, of $C_8H_{16}O$ (ΔH_{Ads}, ΔS_{Ads}) to framework Ti atoms are 19 kJ mol^{-1} and 75 J mol^{-1} K^{-1} more positive on nearly defect-free Ti-BEA than those containing ~5 $(SiOH)_4$ (unit cell)$^{-1}$ in the presence of H_2O. Under anhydrous conditions, however, values of ΔH_{Ads} and ΔS_{Ads} do not depend on the density of $(SiOH)_4$. Silanol nests stabilize semiordered clusters of H_2O that must reorganize to accommodate the adsorption of $C_8H_{16}O$. These differences in adsorption thermodynamics result from the short-range interactions between adsorbed $C_8H_{16}O$ and clusters of H_2O that are proximate to Ti active sites. Additionally, the interaction between the aliphatic tail of bound $C_8H_{16}O$ and nearby H_2O molecules increase the entropy of the surrounding solvent structures to a greater extent than observed for the disruption of hydrogen bonds within bulk H_2O. Comparisons of in situ infrared spectra show that the extent of hydrogen bonding among intraporous H_2O molecules decreases significantly in the presence of $C_8H_{16}O$ bound to Ti atoms in hydrophilic Ti-BEA; yet, there is no observable difference in the vibrational features associated with hydrogen-bonded H_2O within hydrophobic materials. These differences further suggest that $C_8H_{16}O$ disrupts stable clusters of H_2O present at proximate $(SiOH)_4$. Within defect-free Ti-BEA, however, intraporous H_2O molecules are not localized near Ti active sites and do respond to the formation of stable Ti-bound adducts. The interactions between the octyl chain of adsorbed $C_8H_{16}O$ and proximate solvent structures form a linear free energy relationship with the associated reorganization of H_2O that occurs during the epoxidation of 1-octene. Collectively, the data and interpretations presented here show that intentional changes in the chemical functionality of micropores can be used to control the interactions between proximate solvent structures and surface intermediates that are critical to both catalysis and adsorption processes.

2. MATERIALS AND METHODS

2.1. Ti-BEA Synthesis. Ti-BEA-*X*, where *X* refers to the initial Si:Al ratio of the parent Al-BEA (*X* = 12.5−250), catalysts were prepared by postsynthetic modification of commercial Al-BEA samples. Al-BEA was treated in refluxing HNO_3 (Macron Chemicals, 68−70 wt %, 20 cm^3 g^{-1}; *Caution: HNO_3 is extremely caustic and will readily cause a chemical burn and should be handled carefully*) with the intent to remove framework Al atoms by forming soluble $Al(NO_3)_3$. The solids were then recovered by vacuum filtration and washed with H_2O (17.8 MΩ·cm, 50 cm^3 g^{-1}) followed by heating at 5 K min^{-1} in flowing air (100 cm^3 min^{-1}) and holding at 823 K for 6 h to remove residual volatile and organic species and to produce Si-BEA-*X*. Materials produced in this manner possessed Si:Al ratios greater than 1400, as determined by energy dispersive X-ray fluorescence spectroscopy. Ti atoms were incorporated by combining a stirred suspension of Si-BEA-*X* in CH_2Cl_2 (Fisher Chemicals, Certified ACS Stabilized) with an appropriate amount of $TiCl_4$ (Sigma-Aldrich, 99.9%; *Caution: $TiCl_4$ will violently react with moisture in the air to form HCl and should be handled carefully*) at reflux. All volatile components were then removed by rotary evaporation. The recovered solids were light-brown, and these materials were treated by heating in flowing air (100 cm^3 min^{-1}) at 5 K min^{-1} and holding at 823 K for 6 h, which produced bright white solid powders.

Ti-BEA-*F* was synthesized hydrothermally in fluoride media by adapting a previously published procedure.[25,40] Briefly, tetraethylammonium fluoride (TEAF, Alfa Aesar, 97 wt %) was dissolved in deionized H_2O (18.2 MΩ·cm) in a polypropylene container and combined with titanium(IV) isopropoxide (TIPO, Sigma-Aldrich, 99.999%) to produce a clear homogeneous solution. Tetraethylorthosilicate (TEOS, Sigma-Aldrich, > 98 wt %) was then added dropwise over a period of 1 min to this solution, which formed a biphasic mixture initially. The mixture was then stirred for 16 h to produce an opaque homogeneous solution. The cover was then removed to evaporate the ethanol and isopropanol that form through the hydrolysis of the TEOS and TIPO, respectively. To ensure that the alcohols were completely removed, an additional 15 wt % of the calculated mass of the alcohols produced was evaporated from the solution. Subsequently, deionized H_2O was added to yield a gel with a final molar composition of 1 SiO_2:0.0033 TIPO: 0.56 TEAF: 7 H_2O. *Note: this synthesis procedure leads to MFI formation when the ethanol and isopropanol are not entirely evaporated.* This gel was then loaded into a Teflon-lined stainless-steel autoclave (Parr instruments, 45 cm^3) that contained 5% (relative to SiO_2 within the gel) dealuminated BEA (Zeolyst, Si:Al = 12.5, see above) as seeds to promote the formation of the BEA zeolite. This autoclave was then heated to 413 K while rotating (60 rpm) in a convection oven for 25 days. The resultant solids were recovered, washed with H_2O and dried for 16 h at 373 K. The dried solids were then heated in flowing air (100 cm^3 min^{-1}) at 823 K (1 K min^{-1}) for 10 h to produce a bleached-white solid.

2.2. Ti-BEA Characterization. The Ti-BEA-*X* materials (created by postsynthetic modification) were used within a previous study,[4] and the detailed chemical and physical characterization of these materials has been described there.

The metal contents of Ti-BEA-*X* were quantified using energy dispersive X-ray fluorescence. Briefly, ~30 mg of Ti-BEA was loaded into a polypropylene sample holder (1 cm diameter) that was sealed with ultralene film. These samples were loaded into a spectrometer (Shimadzu, EDX-7000), whose sample chamber was purged with He (Airgas, Ultrazero grade) prior to measurement. Measurements were taken between 0−30 keV (100 scans averaged), and the relative intensities of the fluorescence features of each element were used to calculate the percent, by mass, of each element within the sample. The density of $(SiOH)_4$ per unit cell ($[(SiOH)_4]$, Table 1) were estimated by taking the initial density of Al per unit cell and subtracting the difference due to the incorporation of Ti atoms.

X-ray diffractograms were collected using a diffractometer (Siemens/Bruker, D5000) with a Cu Kα radiation source

DOI: 10.1021/acscatal.9b03323
ACS Catal. 2019, 9, 10951−10962

Table 1. Ti Metal Loadings, Band Edge Energies, Estimated Number of $(SiOH)_4$ Per Unit Cell, and Relative Densities of Hydrogen-Bonded SiOH (ϕ_{IR}) for all Ti-BEA-*X*

sample	Ti content[a] (wt %)	band edge energy[b] (eV)	$[(SiOH)_4]^c$ (unit cell)$^{-1}$	ϕ_{IR}[d]
Ti-BEA-12.5	0.20	4.2	4.8	2.30
Ti-BEA-20	0.34	4.3	2.9	1.90
Ti-BEA-75	0.28	4.2	0.6	1.60
Ti-BEA-150	0.33	4.2	0.2	1.64
Ti-BEA-250	0.42	4.2	0.1	1.26
Ti-BEA-*F*	0.15	4.3	0	0.08

[a]Measured by EDRXF. [b]Determined from leading edge of Tauc plot from DRUV−vis. [c]Estimated based upon Al removed and Ti replaced within the parent Al-BEA-*X*. [d]Determined from FTIR spectra of dehydrated Ti-BEA-*X*.

(0.15418 nm) under ambient conditions. The similarities between the diffraction patterns for all Ti-BEA-*X* (Figure S1 of the Supporting Information, SI) suggests that all samples within this study possess the *BEA framework.

Band edge energies (E_g, Table 1) were measured by diffuse reflectance UV−vis spectroscopy. In short, samples were intimately ground with magnesium oxide (MgO; Sigma-Aldrich, 99.995%) in a 1:10 (Ti-BEA to MgO) by mass ratio. These samples were loaded into a Harrick diffuse-reflectance accessory and spectra were obtained using a spectrophotometer (Agilent, CARY5) with MgO used as the background. All Ti-BEA possess a single UV−vis absorbance feature around 4.5 eV (Figure S2) and band edges that are significantly greater than bulk TiO_2 (~3.2 eV),[48] which suggests that all Ti-BEA within this study contain highly disperse Ti atoms and larger TiO_x aggregates.

Infrared (IR) spectra of dehydrated Ti-BEA-*X* were obtained using a custom-built transmission cell[49] coupled to a Fourier transform-infrared (FTIR) spectrometer (Bruker, Tensor 37) with a liquid-N_2-cooled HgCdTe detector. Catalysts were pressed into self-supporting disks (~60 mg) and placed within the transmission cell, which was assembled using CaF_2 windows and connected to a gas manifold. All materials were first heated to 573 at 10 K min^{-1} and held for at least 3 h in flowing He (50 cm^3 min^{-1}; Airgas, Ultrazero grade) with the intent to desorb water and volatile organics. Spectra (128 scans, 1 cm^{-1}) were obtained at 573 K in flowing He with an empty cell used as the background. Infrared spectra of dehydrated Ti-BEA (Figure S3; Section S1) show distinct ν(O−H) and ν(Si−O−Si) overtone vibrational modes between 3300−3750 cm^{-1} and 1800−2000 cm^{-1}, respectively. The ratios of the integrated areas (Φ_{IR}) for ν(O−H) of $(SiOH)_4$ ($A_{(siOH)4}$ to those for ν(Si−O−Si) ($A_{(Si-O-Si)}$) provide measures of the relative density of $(SiOH)_4$ for each Ti-BEA,

$$\Phi_{IR} = \frac{A_{(SiOH)_4}}{A_{(Si-O-Si)}} \quad (1)$$

Table 1 shows that values of ϕ_{IR} decrease monotonically with the increasing Si:Al ratio of the parent zeolite, which provides a quantitative measure of the density of $(SiOH)_4$ within Ti-BEA samples.

2.3. Isothermal Titration Calorimetry. The heat released upon $C_8H_{16}O$ or H_2O_2 titration onto Ti-BEA-*X* were measured using a calorimeter (TA Instruments, NanoITC) equipped with gold reference and sample cells (V = 176 μL). Titrations were carried out using a 50 μL ITC syringe at 313 K with a stirring rate of 250 rpm. For all measurements, the CH_3CN (Fisher Chemicals, HPLC grade) used was first dried over activated 3 Å molecular sieves for 3 days. The water content of the CH_3CN is estimated to be <0.1 μM,[50] based upon the use of molecular sieves. Briefly, ~30 mg of Ti-BEA-*X* was suspended in 500 μL of CH_3CN (*neat* or with 39 mM H_2O; 18.2 MΩ·cm) via sonication for 20 min and subsequently loaded into the sample cell of the calorimeter, while the reference cell was filled with *neat* CH_3CN for all measurements. The concentration of H_2O (39 mM) was chosen to facilitate comparisons between the free energies of $C_8H_{16}O$ adsorption and the free energies for C_8H_{16} epoxidation (Section 3.3).[4] Solutions of 1,2-epoxyoctane (Sigma-Aldrich, 98%) or H_2O_2 (Fisher Chemicals, 30 wt.% in H_2O) in CH_3CN (*neat* or with 39 mM H_2O) were loaded into the titration syringe and the system was allowed to reach thermal equilibrium for up to 2 h prior to the start of the experiment. Injections of 1 μL were made at regular intervals (5−60 min) in each experiment, which allowed the system to return to the baseline heating rate prior to a subsequent injection. Data analysis was performed within NanoAnalyze (TA Instruments).

Figure 1a and b shows an exemplary real-time ITC thermogram and the corresponding integrated heat (Q) released, respectively, for the adsorption of $C_8H_{16}O$ onto Ti-BEA-75 in anhydrous CH_3CN. Adsorption enthalpies (ΔH_{Ads}) were determined by averaging the integrated heats for $C_8H_{16}O$ (or H_2O_2) titration onto Ti-BEA-*X* at low coverages (<0.2 (mol titrant)(mol Ti)$^{-1}$), and reported uncertainties in ΔH_{Ads} were calculated from a single standard deviation among these points. Values of the adsorption entropies (ΔS_{Ads}) were calculated by fitting a single-site binding model (Section S2.1) to full-coverage integrated heat data (Section 3.1) while constraining values of ΔH_{Ads} to equal those determined from low-coverage adsorption isotherms. Liquid-phase adsorption within confined environments is complex and reflects charge transfer between the adsorbate and the adsorption site, dispersive interactions with the pore walls, and the solvent reorganization required upon adsorption. The model used to determine values of ΔS_{Ads} (Section S2.1) assumes that all active sites are equivalent, and by extension that all adsorption events involve the same degree of charge transfer, dispersive interactions, and solvent reorganization. These assumptions are necessary to determine values of ΔS_{Ads}, yet the Ti-BEA materials contain Ti active sites with a distribution of proximities from silanol nests and resulting hydrogen bonding interactions. Consequently, differences in ΔS_{Ads} (and ΔH_{Ads}) values across this series of Ti-BEA-*X* reflect how systematic changes in the physical properties of these materials affect these ensemble-averaged values. These full-coverage adsorption isotherms were obtained by combining the integrated heat data from low-coverage (<0.2 (mol $C_8H_{16}O$)(mol Ti)$^{-1}$) experiments with those from high-coverage (0.2−2 (mol $C_8H_{16}O$)(mol Ti)$^{-1}$). All ITC integrated heat data were corrected for the heats of mixing at infinite dilution (see Section S2.2 for details).

2.4. In Situ Attenuated Total Reflection Infrared Spectroscopy and Modulation Excitation. Attenuated total reflectance infrared (ATR-IR) spectroscopy was used to characterize the vibrational structure of H_2O located within the pores of Ti-BEA samples with different densities of $(SiOH)_4$. A given Ti-BEA (~30 mg) was first dispersed into CH_3CN (~1

DOI: 10.1021/acscatal.9b03323
ACS Catal. 2019, 9, 10951−10962

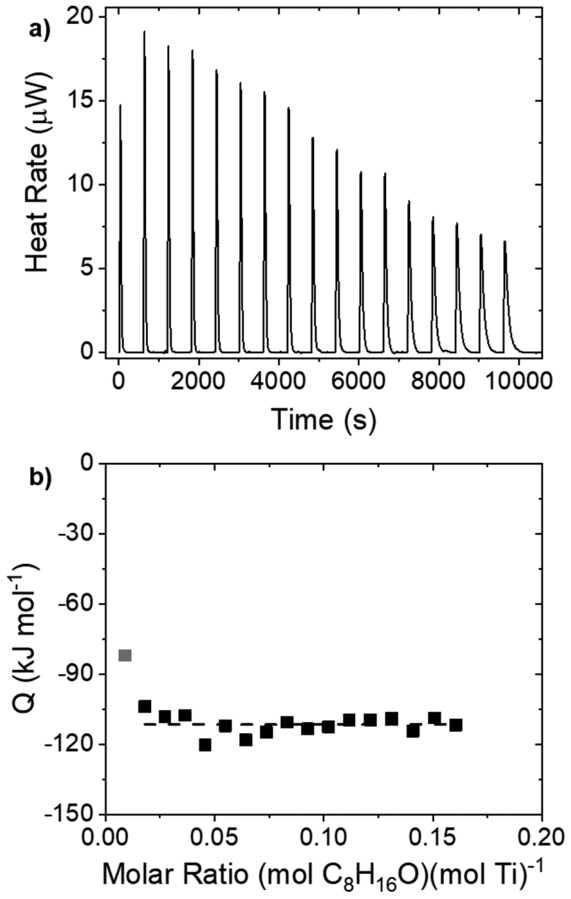

Figure 1. Representative (a) real-time ITC thermogram for the titration of Ti-BEA-75 with $C_8H_{16}O$(5 mM $C_8H_{16}O$, anhydrous CH_3CN), and (b) corresponding heat released (Q) as a function of $C_8H_{16}O$-to-Ti molar ratio. The transparent point was omitted from the calculation of the adsorption enthalpy (denoted by dashed line), due to common errors associated with early injections.

cm^3) via sonication and was drip coated onto a ZnSe cylindrical internal reflection element (IRE; International Crystal Laboratories). The catalyst-coated IRE was loaded into an ATR flow cell (Axiom, TNL-120), which was mounted onto a Fourier-transform infrared spectrometer (Bruker, Vertex 70). Two high-pressure piston pumps (SSI, Series 1) were used to introduce H_2O and CH_3CN solutions and were controlled using LabView. The cell was heated by a resistive heating cartridge placed within the wall of the cell, which was controlled by an electronic temperature controller (Watlow, EZ-Zone). IR spectra (128 scans, 4 cm^{-1} resolution) were obtained continuously during the modulation of H_2O. Background spectra were obtained in *neat* CH_3CN (1 cm^3 min^{-1}, 313 K).

Modulation excitation spectroscopy (MES) uses a periodic stimulation and continuous acquisition of spectra throughout time to obtain time-resolved structural information with high signal-to-noise ratios. Time domain responses are converted to the phase domain, and the spectral changes that occur at the frequency of the applied stimulation are extracted using a phase sensitive detection (PSD) method described by the following equation:

$$A_k(\varphi_k^{\mathrm{PSD}}) = \frac{2}{T}\int_0^T A(t)\sin(k\omega t + \varphi_k^{\mathrm{PSD}})\,\mathrm{d}t \qquad (2)$$

where $A(t)$ and $A_k(\varphi_k^{\mathrm{PSD}})$ are time- and phase-domain responses of the active species respectively, T is the length of a period, ω is the demodulation index, k is the demodulation index (with value of one), and φ_k^{PSD} is the user-defined phase demodulation angle. The application of the MES-PSD technique to FTIR spectra of intermediates on catalytic surfaces greatly increases the signal-to-noise ratio, suppresses the spectral contributions of static (i.e., spectator) species, and reveals high quality spectra containing contributions only of species that change during modulation.[51]

The concentration of H_2O (0−5.5 M) within CH_3CN was modulated sinusoidally by controlling the flow rate of liquid through the two piston pumps such that the set points of the pumps were changed in a stepwise manner every 0.5 s to approximate a sine wave with the desired period. The period length was determined by H_2O cutoff experiments (i.e., switch to anhydrous CH_3CN from 5.5 M H_2O), where the time needed to achieve a ∼95% attenuation of H_2O vibrational features was used as the period length for modulations. The total flow rate was kept at 1 cm^3 min^{-1} by setting the two piston pumps perfectly out of phase with one another. Spectra (4 cm^{-1} resolution, 128 scans; Figure S5) were acquired continuously over 3 h, averaged to a single period, and subsequently converted to the phase domain using eq 1 (Figure S6). The concentration of 5.5 M H_2O was chosen for ATR-IR experiments, because the lower concentrations of 39 mM used in ITC experiments (Section 3.1) and in C_8H_{16} epoxidation reactions (Section 3.3) resulted in IR spectra that had very low signal-to-noise ratios (less than 2−3). Turnover rates for C_8H_{16} epoxidation in Ti-BEA do not depend on the concentration of H_2O at these conditions,[4] and therefore, the thermodynamics of $C_8H_{16}O$ adsorption and kinetics of C_8H_{16} epoxidation (Section 3.3) are unlikely to differ at the concentrations of H_2O used for ATR-IR measurements. These proposals are supported by the similarities between measured values of ΔH_{Ads} for $C_8H_{16}O$ onto Ti-BEA-12.5 within 39 mM H_2O in CH_3CN (−95 ± 2 kJ mol^{-1}) and in 5.5 M H_2O in CH_3CN (−91 ± 4 kJ mol^{-1}).

Phase resolved spectra were then subjected to multivariate curve resolution-alternating least-squares (MCR-ALS) to extract the spectral contributions of independent species.[52] Singular value decomposition show that the combination of two independent species fully describes the phase resolved spectra in all cases. Two sine wave functions were used as initial guesses for time dependent concentrations of species, and the spectra were constrained to solve for positive features. The MATLAB program iteratively solved for spectra and surface coverages until the convergence criteria were met and the sum of residuals was less than 10^{-6}. The resulting spectra were normalized to the most intense ν(O−H) feature using OriginPro 9 software. In all cases, greater than 95% of the variance of the phase-resolved spectra was described by a single component, which implies this component represents the H_2O that enters the pores of Ti-BEA during the modulation experiments.

3. RESULTS AND DISCUSSION

3.1. Effects of Proximate Solvent Structure on Adsorbate Stability. Isothermal titration calorimetry was used to understand how the presence, proximity, and density of $(SiOH)_4$ affects the stability of the $C_8H_{16}O$ bound to Ti active sites. Figure 2a and b shows the integrated heats (Q) released upon titration of Ti-BEA with $C_8H_{16}O$ within aqueous

DOI: 10.1021/acscatal.9b03323
ACS Catal. 2019, 9, 10951−10962

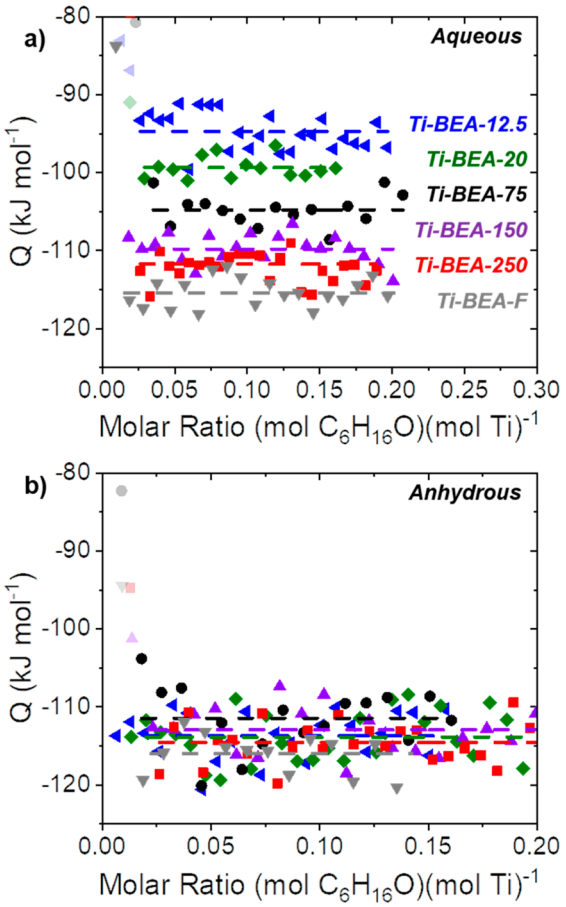

Figure 2. Heats released upon $C_8H_{16}O$ titration onto Ti-BEA as a function of $C_8H_{16}O$:Ti molar ratio in (a) aqueous CH_3CN (39 mM H_2O) and (b) anhydrous CH_3CN. Dashed lines represent the averaged values of Δ. The transparent points were omitted from calculations of Δ, due to common errors associated with early ITC injections. The colored symbols correspond to Ti-BEA-12.5 (blue ◀), Ti-BEA-20 (green ♦), Ti-BEA-75 (black ●), Ti-BEA-150 (purple ▲), Ti-BEA-250 (red ■), and Ti-BEA-*F* (gray ▼).

CH_3CN (39 mM H_2O) and anhydrous CH_3CN, respectively. In all cases, values of *Q* remain constant at low coverages (<0.2 (mol $C_8H_{16}O$)(mol Ti)$^{-1}$), which suggests that these values represent the isosteric adsorption enthalpies (ΔH_{Ads}) at differential coverage. Table 2 shows that values of ΔH_{Ads} are 19 kJ mol^{-1} larger on the most hydrophobic Ti-BEA (Ti-BEA-*F*) than on the most hydrophilic material (Ti-BEA-12.5) when a small amount of H_2O is present ($\Delta H_{Ads,Aq}$; Table 2; Figure 2a). In contrast, values of ΔH_{Ads} for all T-BEA are indistinguishable within anhydrous CH_3CN ($\Delta H_{Ads,Anh}$; Table 2; Figure 2b). These comparisons suggest that silanol nests ($(SiOH)_4$) present within Ti-BEA do not influence the stability of surface-bound intermediates in the absence ofH_2O molecules. The presence of H_2O, however, is required to mediate the interaction between $(SiOH)_4$ and Ti-bound species, which is observed experimentally by measurable changes in $\Delta H_{Ads,Aq}$.

Figure 3a and b shows representative full-coverage isotherms for the titration of Ti active sites with $C_8H_{16}O$ over Ti-BEA-12.5 and Ti-BEA-*F*, respectively. At low coverages (<0.2 (mol $C_8H_{16}O$)(mol Ti)$^{-1}$), the heats released upon incremental titration of Ti atoms are nearly constant (vide infra). As additional $C_8H_{16}O$ is introduced, the heat released per injection decreases with an inflection point centered around a molar ratio of $C_8H_{16}O$ to Ti equal to one, which indicates that each Ti atom binds an average of one $C_8H_{16}O$ molecule in the limit of full saturation.[53] In the presence of H_2O, values of ΔS_{Ads} are 75 J mol^{-1} K^{-1} more positive in Ti-BEA-12.5 than Ti-BEA-*F* ($\Delta S_{Ads,Aq}$; Table 1). Under anhydrous conditions, however, values of ΔS_{Ads} do not depend on the density of $(SiOH)_4$ within Ti-BEA ($\Delta S_{Ads,Anh}$; Table 1). The dependence of ΔS_{Ads} on the density of $(SiOH)_4$ supports the interpretation developed based upon changes in ΔH_{Ads} (see above) in the presence of H_2O: H_2O molecules must restructure to accommodate the formation of surface species. Quantifying the interactions between H_2O that is stabilized at $(SiOH)_4$ and Ti-bound surface species and understanding what these changes represent molecularly requires a rigorous thermodynamic framework that deconstructs how the stability of the bound complex and the reactant states are affected by the presence and proximity of $(SiOH)_4$.

As depicted in Scheme 1, the measured free energies of adsorption (ΔG_{Ads}) represent the difference in thermodynamic stability of the initial and final states of the adsorption process,

$$\Delta G_{Ads} = G_{C_8H_{16}O\text{-}Ti} - G_{C_8H_{16}O} - G_{Ti} \quad (3)$$

where G_j represents the free energy of species *j* (e.g., adsorbed $C_8H_{16}O$). Analogous equalities describe the quantities that determine ΔH_{Ads} and ΔS_{Ads}. The free energies of each of these species depend on specific interactions at solid−liquid

Table 2. Enthalpies[a] and Entropies[b] of Adsorption of $C_8H_{16}O$ onto Ti-BEA-*X* within Aqueous CH_3CN (39 mM H_2O; $\Delta H_{Ads,Anh}$, $\Delta S_{Ads,Anh}$) and Anhydrous CH_3CN ($\Delta H_{Ads,Anh}$, $\Delta S_{Ads,Anh}$), Excess Enthalpies and Entropies of Adsorption of $C_8H_{16}O$ into Ti-BEA-*X* ($H_{C_8H_{16}O\text{-}Ti}^{\varepsilon}$ abd $S_{C_8H_{16}O\text{-}Ti}^{\varepsilon}$), and Enthalpies of H_2O_2 Adsorption-and-Activation ($\Delta H_{Ads,H_2O_2}$))[a,c]

sample	$\Delta H_{Ads,Aq}$ (kJ mol^{-1})	$\Delta S_{Ads,Aq}$ (J mol^{-1} K^{-1})	$H_{C_8H_{16}O\text{-}Ti}^{\varepsilon}$ (kJ mol^{-1})	$S_{C_8H_{16}O\text{-}Ti}^{\varepsilon}$ (J mol^{-1} K^{-1})	$\Delta H_{Ads,Anh}$ (kJ mol^{-1})	$\Delta S_{Ads,Anh}$ (J mol^{-1} K^{-1})	$\Delta H_{Ads,H_2O_2}$ (kJ mol^{-1})
Ti-BEA-12.5	−95 ± 2	−240 ± 10	19 ± 4	75 ± 14	−114 ± 3	−296 ± 11	−36 ± 6
Ti-BEA-20	−99 ± 3	−250 ± 12	15 ± 5	65 ± 15	−118 ± 3	−300 ± 20	−42 ± 8
Ti-BEA-75	−106 ± 2	−279 ± 8	8 ± 4	36 ± 12	−114 ± 4	−301 ± 15	−39 ± 8
Ti-BEA-150	−110 ± 4	−300 ± 12	4 ± 5	15 ± 15	−113 ± 2	−299 ± 15	−40 ± 4
Ti-BEA-250	−112 ± 4	−312 ± 11	2 ± 5	3 ± 14	−116 ± 4	−292 ± 11	−33 ± 6
Ti-BEA-*F*	−114 ± 4	−315 ± 10	0 ± 4	0 ± 10	−115 ± 3	−300 ± 15	−33 ± 4

[a]Values of ΔH_{Ads} were determined by averaging the integrated heats obtained from low-coverage (<0.2 (mol $C_8H_{16}O$)(mol Ti)$^{-1}$) ITC experiments. [b]Values of ΔS_{Ads} were determined by fitting the single-site independent binding model (Section S2.1) to the combined low- and high-coverage integrated heat data, while constraining the value of ΔH_{Ads} to that determined from low-coverage experiments. [c]H_2O_2 titrations give heats that reflect both adsorption of H_2O_2 and its activation to form Ti-OOH species.[4,23,32,54,55]

DOI: 10.1021/acscatal.9b03323
ACS Catal. 2019, 9, 10951−10962

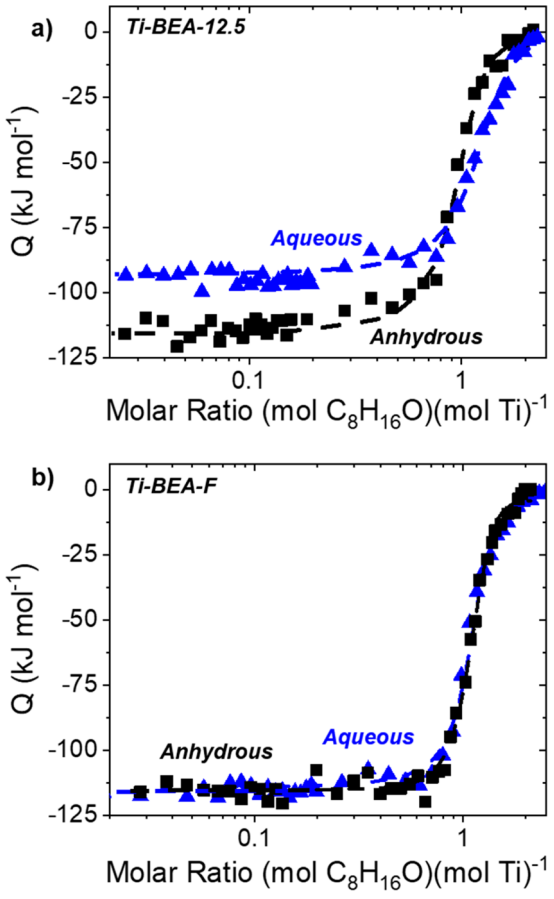

Figure 3. Heats released upon $C_8H_{16}O$ titration onto (a) Ti-BEA-12.5 and (b) Ti-BEA-*F* as a function of $C_8H_{16}O$:Ti molar ratio in aqueous CH_3CN (39 mM H_2O; blue ▲) and anhydrous CH_3CN (black ■). Dashed lines represent fits of a single-site independent binding model (Section S2). Values of *Q* above and below ~0.2 (mol $C_8H_{16}O$)(mol Ti)$^{-1}$ were collected from independent experiments and combined to estimate values of ΔH_{Ads} and ΔS_{Ads}.

interfaces, which can be described as excess free energy contributions (G_j^{ε}).

$$\Delta G_{Ads}|_{Ti\text{-}BEA\text{-}X} = (G_{C_8H_{16}O\text{-}Ti}{}^{o} + G_{C_8H_{16}O\text{-}Ti}{}^{\varepsilon}) - (G_{C_8H_{16}O}{}^{o} + G_{C_8H_{16}O}{}^{\varepsilon}) - (G_{Ti}{}^{o} + G_{Ti}{}^{\varepsilon}) \quad (4)$$

where $\Delta G_{Ads}|_{Ti\text{-}BEA\text{-}X}$ is the free energy of $C_8H_{16}O$ adsorption onto Ti-BEA-*X* and G_j^{o} is the standard-state Gibbs free energy of species *j*, which is selected to be those for the system with the least-significant hydrogen bonding (i.e., G_j^{o} reflects the stability of species within Ti-BEA-*F*).

$$\Delta G_{Ads}|_{Ti\text{-}BEA\text{-}F} = G_{C_8H_{16}O\text{-}Ti}{}^{o} - G_{C_8H_{16}O}{}^{o} - G_{Ti}{}^{o} \quad (5)$$

The value of $G_{C_8H_{16}O}{}^{\varepsilon}$ is negligible, because the activity of the fluid-phase $C_8H_{16}O$ is not affected by the density of $(SiOH)_4$ within the pores of Ti-BEA. Consequently, differences in the adsorption free energies of $C_8H_{16}O$ measured among a given Ti-BEA-*X* and Ti-BEA-*F* ($\Delta\Delta G_{Ads}$) reflect only differences in the excess free energies of adsorbed $C_8H_{16}O$ and the solvent-saturated Ti sites prior to $C_8H_{16}O$ adsorption,

$$\Delta\Delta G_{Ads} = \Delta G_{Ads}|_{Ti\text{-}BEA\text{-}X} - \Delta G_{Ads}|_{Ti\text{-}BEA\text{-}F} = G_{C_8H_{16}O\text{-}Ti}{}^{\varepsilon} - G_{Ti}{}^{\varepsilon} \quad (6)$$

Deconvoluting the individual contributions of $G_{C_8H_{16}O\text{-}Ti}{}^{\varepsilon}$ and G_{Ti}^{ε} and to show how these depend on $[(SiOH)_4]$ requires a calorimetric measurements of a separate, but fundamentally related, adsorption process.

Titrations of Ti atoms with H_2O_2 involves the adsorption and activation of H_2O_2 to form the Ti-OOH intermediates that form and react with alkenes during epoxidations.[4,23,32,54−59] Accordingly, the measured free energies of H_2O_2 adsorption-and-activation ($\Delta G_{Ads,H_2O_2}$) are given by the following:

$$\Delta G_{Ads,H_2O_2} = (G_{Ti\text{-}OOH}{}^{o} + G_{Ti\text{-}OOH}{}^{\varepsilon}) - (G_{H_2O_2}{}^{o} + G_{H_2O_2}{}^{\varepsilon}) - (G_{Ti}{}^{o} + G_{Ti}{}^{\varepsilon}) \quad (7)$$

where nomenclature follows that defined above. Values of $\Delta H_{Ads,H_2O_2}$ (Table 1) do not depend on $[(SiOH)_4]$, which suggests that either $H_{Ti\text{-}OOH}^{\varepsilon}$ and H_{Ti}^{ε} are coincidentally equal and opposite in magnitude or that neither vary with $[(SiOH)_4]$, which seems more probable across the set of six materials.[60] The apparent independence of $H_{Ti\text{-}OOH}^{\varepsilon}$ with $[(SiOH)_4]$ reflects the tendency for Ti-OOH to donate and accept hydrogen bonds and spontaneously stabilize H_2O,[61,62] which obviates the differences introduced by the presence of H_2O held at nearby $(SiOH)_4$. Prior to titration with $C_8H_{16}O$, titanium atoms in all Ti-BEA are coordinated to solvent molecules (i.e., CH_3CN), which suggests that the initial state of the Ti active sites are not affected by proximate H_2O in materials with varying $[(SiOH)_4]$. Consequently, the measured values of $\Delta G_{Ads,H_2O_2}$ suggest that $\Delta\Delta G_{Ads}$ among Ti-BEA materials reflect only the manner in which values of $G_{C_8H_{16}O\text{-}Ti}{}^{\varepsilon}$ depend on $[(SiOH)_4]$ and the H_2O clusters that nearby defects stabilize. Monte Carlo simulations for H_2O adsorption into silicalite-1 with varying densities of $(SiOH)_4$ (0.125−4 (unit cell)$^{-1}$) show that the low-coverage heats of adsorption for H_2O onto $(SiOH)_4$ are independent of $(SiOH)_4$ density.[63] Therefore, measured changes in $G_{C_8H_{16}O\text{-}Ti}{}^{\varepsilon}$ do not reflect differences in the stability of H_2O within different Ti-BEA-*X*; rather, values of $G_{C_0H_{16}O\text{-}Ti}{}^{\varepsilon}$ reflect the interactions between $C_8H_{16}O$ and H_2O stabilized at $(SiOH)_4$, where the magnitude of these values depends critically on the likelihood that a $(SiOH)_4$ is near the Ti active sites. The apparent independent behavior between Ti atoms and nearby $(SiOH)_4$ within hydrophilic Ti-BEA under anhydrous conditions may be attributed to the nonpolar chemical functionality of adsorbed $C_8H_{16}O$ or manifests from the molecular length of $C_8H_{16}O$. Adsorbates that are sufficiently long or possess hydrogen bond-donating or -accepting functional groups may interact with nearby $(SiOH)_4$, even within anhydrous conditions, such that the thermodynamic stability of these adsorbates may possess a measurable dependence on $[(SiOH)_4]$. In short, the differences in the thermodynamics of adsorption directly report on the outer-sphere interactions between adsorbed species and the extended surface of the zeolite that are mediated by the solvent structures confined within these voids.

3.2. Spectroscopic Evidence for the Disruption of Hydrogen Bonds. In situ attenuated total reflectance-infrared spectroscopy (ATR-IR) in conjunction with modulation excitation provides direct evidence for the interactions between confined H_2O and hydrophobic surface species (i.e., adsorbed $C_8H_{16}O$). Figure 4 shows the extracted spectra of intermediates in Ti-BEA-12.5 (Figure 4a), Ti-BEA-250 (Figure 4b), and Ti-BEA-*F* (Figure 4c), during modulation of H_2O in the presence and absence of $C_8H_{16}O$; these features reflect the

DOI: 10.1021/acscatal.9b03323
ACS Catal. 2019, 9, 10951−10962

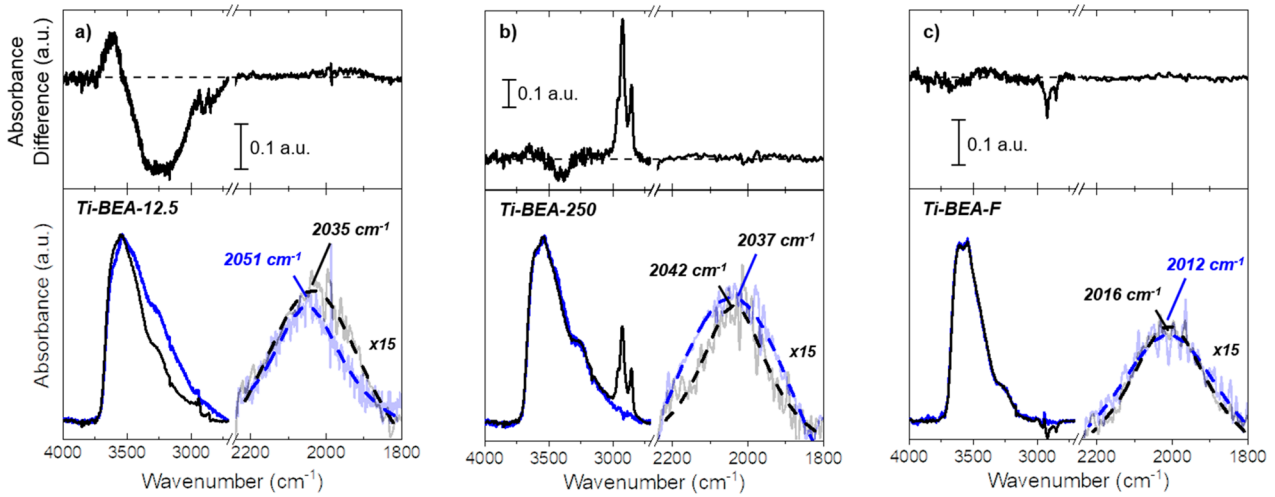

Figure 4. Infrared spectra obtained through multivariate analysis of modulation excitation experiments (Section 2.4) of H_2O in CH_3CN (0−5.5 M H_2O; blue) and in a solution of $C_8H_{16}O$ in CH_3CN (0.1 M $C_8H_{16}O$, 0−5.5 M H_2O; black) over: a) Ti-BEA-12.5, b) Ti-BEA-250, and c) Ti-BEA-*F*. All spectra are normalized to the most-intense ν(O−H) feature (~3540 cm^{-1}) and have a resolution of 5 cm^{-1}. The region between 1800−2250 cm^{-1} have been scaled by a factor of 15. The dashed curves represent Lorentzian fits, which were used to quantify the peak center of the combination band. The top spectra for each panel is the difference spectra that represents that changes in the vibrational features for H_2O that result from the presence of $C_8H_{16}O$.

spectral contributions that change because H_2O molecules enter the pores of each Ti-BEA. The corresponding difference spectra are shown in the top panels within Figure 4 to more-clearly depict those features that change in response to adsorbed $C_8H_{16}O$ and to facilitate comparisons among different Ti-BEA samples. The absorbance features at ~2050 cm^{-1} and between 3000 and 3750 cm^{-1} correspond to the combination (bending+libration) mode of H_2O molecules and the stretching of hydroxyl groups (ν(O−H)), respectively.[64] Features near 2950 cm^{-1} correspond to ν(C−H) of the methyl and methylene units of $C_8H_{16}O$.[65] Within Ti-BEA-250 there is a prominent ν(C−H) in the presence of $C_8H_{16}O$, which likely arises from small differences in the concentration of $C_8H_{16}O$ in the two solutions during modulation of H_2O. Notably, this cannot be attributed to the expulsion of $C_8H_{16}O$ from Ti-BEA due to the introduction of H_2O, as this would result in a negative absorbance feature.

Coordination of the epoxide to framework Ti atoms results in distinct changes in the structure of the aqueous solvent, and the extent of these differences depend on the density of silanol groups in Ti-BEA and their proximity to Ti sites. In Ti-BEA-12.5, the presence of $C_8H_{16}O$ leads to a significant loss in intensity of ν(O−H) around 3250 cm^{-1} and a simultaneous increase in intensity near 3700 cm^{-1}, which are consistent with expectations for spectral differences caused by a decrease in the average number of hydrogen bonds among H_2O molecules near active sites. Moreover, the combination band (~2050 cm^{-1}) shifts to lower wavenumbers, which reflects lower barriers for librations of individual H_2O molecules within their environments, another indication of diminished hydrogen bonding.[64] In contrast, spectra obtained from hydrophobic Ti-BEA-250 (Figure 4b) and Ti-BEA-*F* (Figure 4c) do not show any differences in features corresponding to ν(O−H) or to combination modes for H_2O associated with the presence of adsorbed $C_8H_{16}O$. These similarities suggest that the small amounts of H_2O located within the pores do not interact with epoxide bound to Ti atoms, presumably because H_2O molecules are not stabilized as clusters near the Ti sites by interactions with $(SiOH)_4$ groups. This interpretation is further supported by the reduced intensity of the ν(O−H) band at lower wavenumbers (~3250 cm^{-1}) of both Ti-BEA-250 and Ti-BEA-*F*, in comparison to Ti-BEA-12.5, which indicates that the H_2O within these hydrophobic materials possess fewer hydrogen bonds than those within Ti-BEA-12.5. Notably, the spectrum of H_2O within Ti-BEA-250 shows slightly greater absorbance near 3250 cm^{-1} that that of Ti-BEA-*F* and suggests a greater extent of hydrogen bonding likely caused by residual silanol nests or defects introduced by the postsynthetic modification procedure. Despite the presences of these surface functions, the vibrational modes H_2O are not affected by the presence of $C_8H_{16}O$, which demonstrates that H_2O molecules within Ti-BEA-250 are too far from active sites to be influenced by adsorption of $C_8H_{16}O$ to Ti atoms. Spectra from the clean ZnSe internal reflection element (Figure S7) exhibit no change in ν(O−H) or shift in the combination band of H_2O in the presence of $C_8H_{16}O$, which further demonstrates the differences within spectra from Ti-BEA samples arise from the interactions among H_2O and $C_8H_{16}O$ at the framework Ti atoms within the zeolites and not from the bulk solution.

3.3. Linear Free Energy Relationships Describe Solvent Reorganization at the Solid−Liquid Interface.

Calorimetric and spectroscopic results strongly suggest that molecular interactions between the hydrophobic chain of adsorbed $C_8H_{16}O$ and nearby clusters of H_2O molecules stabilized by $(SiOH)_4$ structures cause $H_{C_8H_{16}O\text{-}Ti}^{\varepsilon}$ and $S_{C8H^{16}O\text{-}Ti}^{\varepsilon}$ values (Table 2) to depend strongly on the density of $(SiOH)_4$ in Ti-BEA (Table 1). These differences indicate that $C_8H_{16}O$ bound to Ti atoms within hydrophobic Ti-BEA materials (Ti-BEA-*F*, Ti-BEA-250) interact primarily with intraporous CH_3CN, because the nearly pristine siloxane pores contain negligible amounts of H_2O near Ti atoms. In contrast, the more hydrophilic Ti-BEA materials (e.g., Ti-BEA-12.5) contain multiple $(SiOH)_4$ groups per unit cell which anchor clusters of H_2O near Ti active sites. These H_2O clusters (and nearby CH_3CN molecules) restructure to accommodate adsorbed $C_8H_{16}O$, which incurs an enthalpic penalty from

DOI: 10.1021/acscatal.9b03323
ACS Catal. 2019, 9, 10951−10962

the disruption of hydrogen bonds (i.e., $\Delta H_{Ads,Aq}$ increases with $[(SiOH)_4]$ due to differences in $H_{C_8H_{16}O\text{-}Ti}^{\varepsilon}$; Table 1). These solvent-adsorbate interactions result also in large positive values of $S_{C_8H_{16}O\text{-}Ti}^{\varepsilon}$ generated by the reorganization of confined H_2O clusters.

The changes in $H_{C_8H_{16}O\text{-}Ti}^{\varepsilon}$ and $S_{C_8H_{16}O\text{-}Ti}^{\varepsilon}$ that increase with $[(SiOH)_4]$ (Table 1) are qualitatively consistent with the expected enthalpy and entropy changes associated with disrupting hydrogen bonds within bulk H_2O. The breaking of a single hydrogen bond within liquid water by interaction with a nonpolar solute increases the enthalpy of the system by ~8 kJ mol^{-1} and results in a concomitant increase in entropy of ~20 J mol^{-1} K^{-1}.[66,67] Figure 5 shows the relationships

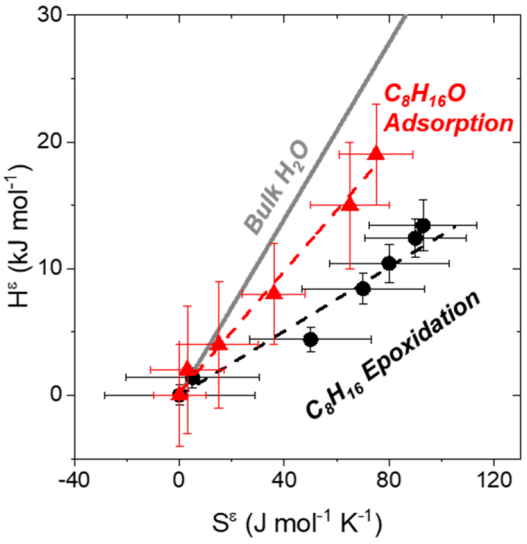

Figure 5. Excess enthalpiesas a function of excess entropies for C_8H_{16} epoxidation transition states (black ●; i.e., $H^{\ddagger,\varepsilon}$ and $S^{\ddagger,\varepsilon}$) and $C_8H_{16}O$-Ti (red ▲; i.e.,$H_{C_8H_{16}O\text{-}Ti}^{\varepsilon}$ and $G_{C_8H_{16}O\text{-}Ti}^{\varepsilon}$). The dashed lines represent linear fits to the data and the bold gray line represents the enthalpy–entropy compensation effect that describes changes in hydrogen bonding within bulk H_2O (e.g., by solvating a nonpolar solute).[66]

between excess enthalpies and the commensurate excess entropies that describe the restructuring of H_2O clusters to accommodate C_8H_{16} epoxidation transition states ($H^{\ddagger,\varepsilon}$ and $S^{\ddagger,\varepsilon}$) and adsorbed $C_8H_{16}O$ ($H_{C_8H_{16}O\text{-}Ti}^{\varepsilon}$ and $S_{C_8H_{16}O\text{-}Ti}^{\varepsilon}$) together with the corresponding enthalpy–entropy compensation effects for hydrogen bonding in bulk water. Water confined within nanopores (e.g., within Ti-BEA) possess significantly lower entropies than bulk H_2O,[68−70] which suggests that disruption of confined H_2O structures should result in a larger entropy gain and smaller enthalpy cost relative to that observed in bulk H_2O. The greater entropic compensation for the disruption of H_2O confined within Ti-BEA results from the reduced dimensionality of the H_2O molecules. These micropores (~0.65 Å diameter) cannot accommodate the tetrahedral coordination and three-dimensions of hydrogen-bonding that H_2O molecules possess in bulk solutions. Therefore, the entropy gained upon disrupting these hydrogen-bonding interactions is greater within Ti-BEA, because fewer hydrogen bonds must be broken to destabilize (or "free") each H_2O molecule.

Figure 6a and b show that the excess enthalpies and entropies for $C_8H_{16}O$ epoxidation transition states ($H^{\ddagger,\varepsilon}$ and

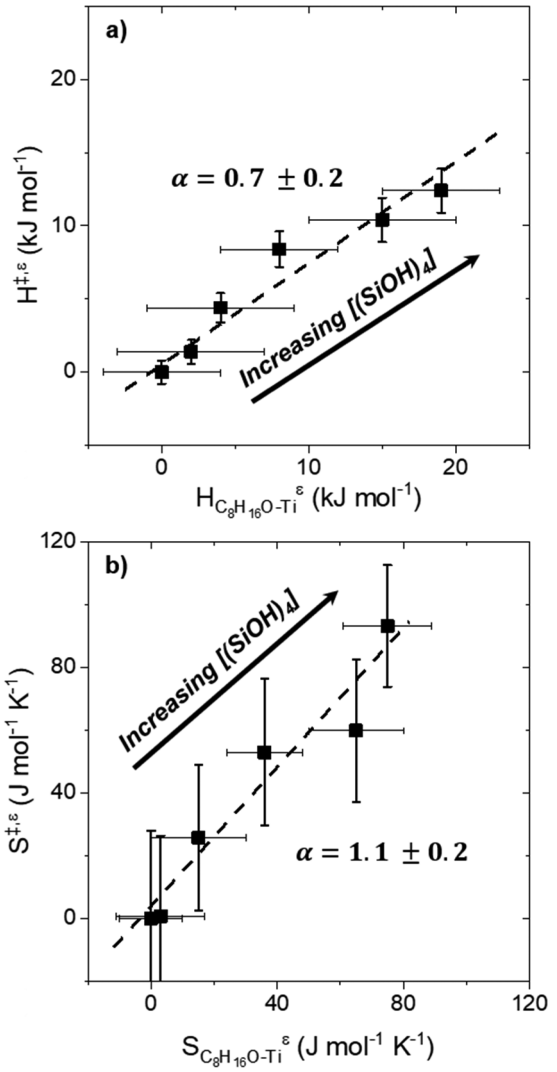

Figure 6. (a) Excess enthalpies and (b) excess entropies for C_8H_{16} epoxidation ($H^{\ddagger,\varepsilon}$ and $S^{\ddagger,\varepsilon}$) as a function of $C_8H_{16}O$ adsorption ($H_{C_8H_{16}O\text{-}Ti}^{\varepsilon}$ and $S_{C_8H_{16}O\text{-}Ti}^{\varepsilon}$,) over Ti-BEA-*X*, respectively. The bold gray line represents parity and the dashed lines are linear fits to the data, where the slope of these fits are indicated by the values of α.

$S^{\ddagger,\varepsilon}$; 0.1 mM C_8H_{16}, 0.01 M H_2O_2, 0.039 M H_2O, in CH_3CN, 313 K)[4] increase linearly as a function of the respective excess enthalpies and entropies for $C_8H_{16}O$ adsorption ($H_{C_8H_{16}O\text{-}Ti}^{\varepsilon}$ and $S_{C_8H_{16}O\text{-}Ti}^{\varepsilon}$). These values exhibit a strong linear free energy relationship (LFER) that suggests that the outer-sphere interactions that affect the stability of C_8H_{16} epoxidation transition states are chemically similar to those that affect $C_8H_{16}O$ adsorption.[71,72] Linear free energy relationships for elementary steps in catalysis commonly follow the form,[72]

$$\Delta G^{\ddagger} = \alpha \times \Delta G_{Ads} + \beta \quad (8)$$

where $\Delta G^{\ddagger}$ describes the activation free energy for an elementary step (e.g., reaction of Ti-OOH with an alkene), ΔG_{Ads} is the free energy change corresponding to the step, α is the similarity (or transmission) coefficient, and β is a constant representing an intrinsic activation barrier for the elementary step. The LFERs shown in Figure 6 describe the endothermic changes in solvent structure (see comparisons within Table 2) that are associated with the perturbation of H_2O proximate to

DOI: 10.1021/acscatal.9b03323
ACS Catal. 2019, 9, 10951−10962

Ti active sites upon formation of the C_8H_{16} epoxidation transition states or upon $C_8H_{16}O$ adsorption. These comparisons between thermodynamic and kinetic parameters (i.e., with similarity coefficients that approach unity) show that the differences in hydrogen bonding within nearby H_2O clusters affect the stability of adsorbed $C_8H_{16}O$ in ways that strongly resemble their influence on the stability of 1-octene epoxidation transition states, because the values of the excess contributions of these specific interactions are proportional (e.g., $H_{C_8H_{16}O\text{-}Ti}^{\varepsilon} \sim H^{\ddagger,\varepsilon}$) and similar in Ti-BEA.

In short, the analysis and interpretation of results show that the excess free energies of surface intermediates critical to catalysis and adsorption depend intimately on the presence, density, and proximity of hydrogen-bonded solvent structures, which underscores the complexity of solid−liquid interfaces. These findings suggest that interactions between confined solvent structures and reactive species at proximate active sites can be used to change the thermodynamics of adsorption and the kinetics of catalytic reactions. Ongoing work seeks to elucidate how the chemical and physical properties of the pore walls (e.g., zeolite topology) impact the structuring of solvent molecules and the ensuing interactions with surface intermediates.

4. CONCLUSIONS

The thermodynamic stability of surface intermediates critical to catalysis and adsorption depend intimately on the presence, proximity, and density of $(SiOH)_4$ near active sites. Within aqueous solutions of acetonitrile, silanol nests in pores of Ti-BEA nucleate hydrogen-bonded clusters of H_2O that must restructure to accommodate surface intermediates bound to nearby active sites. The reorganization of the solvent results in adsorption enthalpies and entropies for $C_8H_{16}O$ that are 19 and 75 kJ mol^{-1} more-positive in Ti-BEA that contain ∼5 $(SiOH)_4$ (unit cell)$^{-1}$ than those for defect-free materials. These differences, however, become negligible under anhydrous conditions that fill micropores only with CH_3CN solvent molecules that restructure to similar extents for BEA samples with all $(SiOH)_4$ densities examined: enthalpies and entropies for $C_8H_{16}O$ adsorption are similar across all Ti-BEA samples in the absence of H_2O. The adsorption of $C_8H_{16}O$ disrupts hydrogen-bonding interactions among H_2O molecules in hydrophilic Ti-BEA as demonstrated by a significant loss in the absorbance of ν(O−H) around 3250 cm^{-1} and a red shift in the libration+bending combination band for H_2O molecules. The vibrational spectra of H_2O in the presence or absence of $C_8H_{16}O$ are, however, indistinguishable in defect-free Ti-BEA, which suggests that H_2O molecules that reside within these hydrophobic pores do not interact with species that form at Ti active sites. The excess free energies of adsorption that describe the restructuring of confined H_2O molecules form a linear free energy relationship with the associated excess properties for 1-octene epoxidation transition states, because these excess quantities predominantly reflect the changes in interactions among nearby solvent structures induced by the presence of the octyl chain of these reactive surface intermediates.

Collectively, the data and interpretations presented here demonstrate that complex outer-sphere interactions at solid−liquid interfaces follow linear free energy relationships. Specifically, small confined clusters of hydrogen-bonding solvent molecules (e.g., H_2O or ROH) nucleate at polar functions within extended pores and must reorganize to accommodate the formation of surface intermediates critical to catalysis or adsorption. The reorganization energy typically manifests within excess free energies that depend sensitively on the combination of the chemical and physical properties of the reactant, solvent, and catalyst. These conclusions suggest that chemical modifications of extended solid surfaces can be used to regulate adsorption and catalysis by sets of interactions that are orthogonal to those that control charge transfer at active sites.

■ ASSOCIATED CONTENT

Supporting Information

The Supporting Information is available free of charge on the ACS Publications website at DOI: 10.1021/acscatal.9b03323.

X-ray diffraction, diffuse reflectance UV−vis, infrared spectra of dehydrated Ti-BEA-*X*, ITC binding model derivation, ITC dilution curve, example ATR-IR spectra during MES, and ATR-IR spectra of Ti-BEA-250 (PDF)

■ AUTHOR INFORMATION

Corresponding Author

*E-mail: dwflhrty@illinois.edu.

ORCID

Daniel T. Bregante: 0000-0003-2157-1286

David W. Flaherty: 0000-0002-0567-8481

Notes

The authors declare no competing financial interest.

■ ACKNOWLEDGMENTS

D.T.B. acknowledges helpful discussions Ms. Megan Witzke. D.T.B. was supported by by the United States Department of Defense (DoD) through the National Defense Science & Engineering Graduate (NDSEG) Fellowship program. This work was supported by the U.S. Army Research Office under grant number W911NF-10-1-0100, with partial support from a research grant from the National Science Foundation (CBET-15531377).

■ REFERENCES

(1) Lai, Z.; Bonilla, G.; Diaz, I.; Nery, J. G.; Sujaoti, K.; Amat, M. A.; Kokkoli, E.; Terasaki, O.; Thompson, R. W.; Tsapatsis, M.; et al. Microstructural Optimization of a Zeolite Membrane for Organic Vapor Separation. *Science* **2003**, *300*, 456−460.

(2) Rangnekar, N.; Mittal, N.; Elyassi, B.; Caro, J.; Tsapatsis, M. Zeolite membranes - a review and comparison with MOFs. *Chem. Soc. Rev.* **2015**, *44*, 7128−7154.

(3) Sievers, C.; Noda, Y.; Qi, L.; Albuquerque, E. M.; Rioux, R. M.; Scott, S. L. Phenomena Affecting Catalytic Reactions at Solid-Liquid Interfaces. *ACS Catal.* **2016**, *6*, 8286−8307.

(4) Bregante, D. T.; Johnson, A. M.; Patel, A. Y.; Ayla, E. Z.; Cordon, M. J.; Bukowski, B. C.; Greeley, J.; Gounder, R.; Flaherty, D. W. Cooperative Effects between Hydrophilic Pores and Solvents: Catalytic Consequences of Hydrogen Bonding on Alkene Epoxidation in Zeolites. *J. Am. Chem. Soc.* **2019**, *141*, 7302−7319.

(5) Reichardt, D.; Welton, T. *Solvents and Solvent Effects in Organic Chemistry*, 4th ed., Wiley-VCH: 2010.

(6) Yadav, A.; Jackson, R. M.; Holbrook, J. J.; Warshel, A. Role of Solvent Reorganization Energies in the Catalytic Activity of Enzymes. *J. Am. Chem. Soc.* **1991**, *113*, 4800−4805.

(7) Gould, N. S.; Xu, B. Temperature-Programmed Desorption of Pyridine on Zeolites in the Presence of Liquid Solvents. *ACS Catal.* **2018**, *8*, 8699−8708.

(8) Zhang, K.; Lively, R. P.; Noel, J. D.; Dose, M. E.; McCool, B. A.; Chance, R. R.; Koros, W. J. Adsorption of water and ethanol in MFI-type zeolites. *Langmuir* **2012**, *28*, 8664−73.
(9) Zhang, K.; Lively, R. P.; Dose, M. E.; Brown, A. J.; Zhang, C.; Chung, J.; Nair, S.; Koros, W. J.; Chance, R. R. Alcohol and water adsorption in zeolitic imidazolate frameworks. *Chem. Commun.* **2013**, *49*, 3245−3247.
(10) Shah, D.; Kissick, K.; Ghorpade, A.; Hannah, R.; Bhattacharyya, D. Pervaporation of alcohol-water and dimethylformamide-water mixtures using hydrophilic zeolite NaA membranes: mechanisms and experimental results. *J. Membr. Sci.* **2000**, *179*, 185−205.
(11) Nalaparaju, A.; Zhao, X. S.; Jiang, J. W. Molecular Understanding for the Adsorption of Water and Alcohols in Hydrophilic and Hydrophobic Zeolitic Metal-Organic Frameworks. *J. Phys. Chem. C* **2010**, *114*, 11542−11550.
(12) Lively, R. P.; Dose, M. E.; Thompson, J. A.; McCool, B. A.; Chance, R. R.; Koros, W. J. Ethanol and water adsorption in methanol-derived ZIF-71. *Chem. Commun.* **2011**, *47*, 8667−8669.
(13) Ortiz, A. U.; Freitas, A. P.; Boutin, A.; Fuchs, A. H.; Coudert, F. X. What makes zeolitic imidazolate frameworks hydrophobic or hydrophilic? The impact of geometry and functionalization on water adsorption. *Phys. Chem. Chem. Phys.* **2014**, *16*, 9940−9949.
(14) Cailliez, F.; Stirnemann, G.; Boutin, A.; Demachy, I.; Fuchs, A. H. Does Water Condense in Hydrophobic Cavaties? A Molecular Simulation Study of Hydration in Heterogeneous Nanopores. *J. Phys. Chem. C* **2008**, *112*, 10435−10445.
(15) Trzpit, M.; Soulard, M.; Patarin, J.; Desbiens, N.; Cailliez, F.; Boutin, A.; Demachy, I.; Fuchs, A. H. The Effect of Local Defects on Water adsorption in Silicalite-1 Zeolite: A Joint Experimental and Molecular Simulation Study. *Langmuir* **2007**, *23*, 10131−10139.
(16) Chakraborty, S.; Kumar, H.; Dasgupta, C.; Maiti, P. K. Confined Water: Structure, Dynamics, and Thermodynamics. *Acc. Chem. Res.* **2017**, *50*, 2139−2146.
(17) Majumder, M.; Chopra, N.; Andrews, R.; Hinds, B. J. Enhanced flow in carbon nanotubes. *Nature* **2005**, *438*, 44.
(18) Holt, J. K.; Park, H. G.; Wang, Y.; Stadermann, M.; Artyukhin, A. B.; Grigoropoulos, C. P.; Noy, A.; Bakajin, O. Fast Mass Transport Through Sub-2-Nanometer Carbon Nanotubes. *Science* **2006**, *312*, 1034−1037.
(19) Byl, O.; Liu, J. C.; Wang, Y.; Yim, W. L.; Johnson, J. K.; Yates, J. T. Unusual Hydrogen Bonding in Water-Filled Carbon Nanotubes. *J. Am. Chem. Soc.* **2006**, *128*, 12090−12097.
(20) Thomas, J. A.; McGaughey, A. J. H. Reassessing Fast Water Transport Through Carbon Nanotubes. *Nano Lett.* **2008**, *8*, 2788−2793.
(21) Eckstein, S.; Hintermeier, P. H.; Zhao, R.; Barath, E.; Shi, H.; Liu, Y.; Lercher, J. A. Influence of Hydronium Ions in Zeolites on Sorption. *Angew. Chem., Int. Ed.* **2019**, *58*, 3450−3455.
(22) Wang, M.; Jaegers, N. R.; Lee, M.-S.; Wan, C.; Hu, J. Z.; Shi, H.; Mei, D.; Burton, S. D.; Camaioni, D. M.; Gutierrez, O. Y.; Glezakou, V.-A.; Rousseau, R.; Wang, Y.; Lercher, J. A. Genesis and Stability of Hydronium Ions in Zeolite Channels. *J. Am. Chem. Soc.* **2019**, *141*, 3444−3455.
(23) Bregante, D. T.; Thornburg, N. E.; Notestein, J. M.; Flaherty, D. W. Consequences of Confinement for Alkene Epoxidation with Hydrogen Peroxide on Highly Dispersed Group 4 and 5 Metal Oxide Catalysts. *ACS Catal.* **2018**, *8*, 2995−3010.
(24) Gounder, R. Hydrophobic microporous and mesoporous oxides as Brønsted and Lewis acid catalysts for biomass conversion in liquid water. *Catal. Sci. Technol.* **2014**, *4*, 2877−2886.
(25) Cordon, M. J.; Harris, J. W.; Vega-Vila, J. C.; Bates, J. S.; Kaur, S.; Gupta, M.; Witzke, M. E.; Wegener, E. C.; Miller, J. T.; Flaherty, D. W.; et al. *J. Am. Chem. Soc.* **2018**, *140*, 14244−14266.
(26) Bukowski, B. C.; Bates, J. S.; Gounder, R.; Greeley, J. Defect-Mediated Ordering of Condensed Water Structures in Microporous Zeolites. *Angew. Chem., Int. Ed.* **2019** DOI: 10.1002/anie.201908151.
(27) Conrad, S.; Wolf, P.; Müller, P.; Orsted, H.; Hermans, I. Influence of Hydrophilicity on the Snβ-Catalyzed Baeyer-Villiger Oxidation of Cyclohexanone with Aqueous Hydrogen Peroxide. *ChemCatChem* **2017**, *9*, 175−182.
(28) Wang, L.; Sun, J.; Meng, X.; Zhang, W.; Zhang, J.; Pan, S.; Shen, Z.; Xiao, F. S. A significant enhancement of catalytic activities in oxidation with H_2O_2 over the TS-1 zeolite by adjusting the catalyst wettability. *Chem. Commun.* **2014**, *50*, 2012−2014.
(29) Khouw, C. B.; Dartt, C. B.; Labinger, J. A.; Davis, M. E. Studies on the Catalytic-Oxidation of Alkanes and Alkenes by Titanium Silicates. *J. Catal.* **1994**, *149*, 195−205.
(30) Corma, A.; Esteve, P.; Martínez, A. Solvent Effects during the Oxidation of Olefins and Alcohols with Hydrogen Peroxide on Ti-Beta Catalyst: The Influence of the Hydrophilicity-Hydrophobicity of the Zeolite. *J. Catal.* **1996**, *161*, 11−19.
(31) Grosso-Giordano, N. A.; Schroeder, C.; Okrut, A.; Solovyov, A.; Schottle, C.; Chasse, W.; Marinkovic, N.; Koller, H.; Zones, S. I.; Katz, A. Outer-Sphere Control of Catalysis on Surfaces: A Comparative Study of Ti(IV) Single-Sites Grafted on Amorphous versus Crystalline Silicates for Alkene Epoxidation. *J. Am. Chem. Soc.* **2018**, *140*, 4956−4960.
(32) Bregante, D. T.; Flaherty, D. W. Periodic Trends in Olefin Epoxidation over Group IV and V Framework Substituted Zeolite Catalysts: A Kinetic and Spectroscopic Study. *J. Am. Chem. Soc.* **2017**, *139*, 6888−6898.
(33) Bai, P.; Tsapatsis, M.; Siepmann, J. I. Multicomponent adsorption of alcohols onto silicalite-1 from aqueous solution: isotherms, structural analysis, and assessment of ideal adsorbed solution theory. *Langmuir* **2012**, *28*, 15566−15576.
(34) Wang, C.-H.; Bai, P.; Siepmann, J. I.; Clark, A. E. Deconstructing Hydrogen-Bond Networks in Confined Nanoporous Materials: Implications for Alcohol-Water Separation. *J. Phys. Chem. C* **2014**, *118*, 19723−19732.
(35) Farzaneh, A.; DeJaco, R. F.; Ohlin, L.; Holmgren, A.; Siepmann, J. I.; Grahn, M. Comparative Study of the Effect of Defects on Selective Adsorption of Butanol from Butanol/Water Binary Vapor Mixtures in Silicalite-1 Films. *Langmuir* **2017**, *33*, 8420−8427.
(36) Khouw, C. B.; Dartt, C. B.; Labinger, J. A.; Davis, M. E. Studies on the Catalytic Oxidation of Alkanes and Alkenes by Titanium Silicates. *J. Catal.* **1994**, *149*, 195−205.
(37) Clerici, M. G. The activity of titanium silicalite-1 (TS-1): Some considerations on its origin. *Kinet. Catal.* **2015**, *56*, 450−455.
(38) Gounder, R.; Davis, M. E. Beyond shape selective catalysis with zeolites: Hydrophobic void spaces in zeolites enable catalysis in liquid water. *AIChE J.* **2013**, *59*, 3349−3358.
(39) Wu, L.; Tang, Z.; Yu, Y.; Yao, X.; Liu, W.; Li, L.; Yan, B.; Liu, Y.; He, M. Facile synthesis of a high-performance titanosilicate catalyst with controllable defective $Ti(OSi)_3OH$ sites. *Chem. Commun.* **2018**, *54*, 6384−6387.
(40) Blasco, T.; Camblor, M. A.; Corma, A.; Esteve, P.; Guil, J. M.; Martinez, A.; Perdigon-Melon, J. A.; Valencia, S. Direct synthesis and characterization of hydrophobic aluminum-free Ti-beta zeolite. *J. Phys. Chem. B* **1998**, *102*, 75−88.
(41) Ge, T.; Hua, Z.; Lv, J.; Zhou, J.; Guo, H.; Zhou, J.; Shi, J. Hydrophilicity/hydrophobicity modulated synthesis of nano-crystalline and hierarchically structured TS-1 zeolites. *CrystEngComm* **2017**, *19*, 1370−1376.
(42) Park, S.; Cho, K. M.; Youn, M. H.; Seo, J. G.; Jung, J. C.; Baeck, S.-H.; Kim, T. J.; Chung, Y.-M.; Oh, S.-H.; Song, I. K. Direct epoxidation of propylene with hydrogen peroxide over TS-1 catalysts: Effect of hydrophobicity of the catalysts. *Catal. Commun.* **2008**, *9*, 2485−2488.
(43) Dyson, P. J.; Jessop, P. G. Solvent Effects in Catalysis: Rational Improvements of Catalysts *via* Manipulation of Solvent Effects. *Catal. Sci. Technol.* **2016**, *6*, 3302−3316.
(44) Mellmer, M. A.; Sanpitakseree, C.; Demir, B.; Bai, P.; Ma, K.; Neurock, M.; Dumesic, J. A. Solvent-Enabled Control of Reactivity for Liquid Phase Reactions of Biomass-Derived Compounds. *Nature Catal.* **2018**, *1*, 199−207.

DOI: 10.1021/acscatal.9b03323
ACS Catal. 2019, 9, 10951−10962

(45) Mellmer, M. A.; Sener, C.; Gallo, J. M. R.; Luterbacher, J. S.; Alonso, D. M.; Dumesic, J. A. Solvent Effects in Acid-Catalyzed Biomass Conversion Reactions. *Angew. Chem., Int. Ed.* **2014**, *53*, 11872−11875.
(46) Walker, T. W.; Chew, A. K.; Li, H.; Demir, B.; Zhang, Z. C.; Huber, G. W.; Van Lehn, R. C.; Dumesic, J. A. Universal Kinetic Solvent Effects in Acid-Catalyzed Reactions of Biomass-Derived Oxygenates. *Energy Environ. Sci.* **2018**, *11*, 617−628.
(47) Kalmutzki, M. J.; Diercks, C. S.; Yaghi, O. M. Metal-Organic Frameworks for Water Harvesting from Air. *Adv. Mater.* **2018**, *30*, No. 1704304.
(48) Thornburg, N. E.; Thompson, A. B.; Notestein, J. M. Periodic Trends in Highly Dispersed Groups IV and V Supported Metal Oxide Catalysts for Alkene Epoxidation with H_2O_2. *ACS Catal.* **2015**, *5*, 5077−5088.
(49) Wang, J.; Kispersky, V. F.; Delgass, N. W.; Ribeiro, F. H. Determination of the Au active site and surface active species via operando transmission FTIR and isotopic transient experiments on 2.3wt.% Au/TiO2 for the WGS reaction. *J. Catal.* **2012**, *289*, 171−178.
(50) Williams, D. B.; Lawton, M. Drying of organic solvents: quantitative evaluation of the efficiency of several desiccants. *J. Org. Chem.* **2010**, *75*, 8351−8354.
(51) Urakawa, A.; Bürgi, T.; Baiker, A. Sensitivity enhancement and dynamic behavior analysis by modulation excitation spectroscopy: Principle and application in heterogeneous catalysis. *Chem. Eng. Sci.* **2008**, *63*, 4902−4909.
(52) Jaumot, J.; de Juan, A.; Tauler, R. MCR-ALS GUI 2.0: New features and applications. *Chemom. Intell. Lab. Syst.* **2015**, *140*, 1−12.
(53) Jharimune, S.; Sathe, A. A.; Rioux, R. M. Thermochemical Measurements of Cation Exchange in CdSe Nanocrystals Using Isothermal Titration Calorimetry. *Nano Lett.* **2018**, *18*, 6795−6803.
(54) Bregante, D. T.; Priyadarshini, P.; Flaherty, D. W. Kinetic and spectroscopic evidence for reaction pathways and intermediates for olefin epoxidation on Nb in *BEA. *J. Catal.* **2017**, *348*, 75−89.
(55) Bregante, D. T.; Patel, A. Y.; Johnson, A. M.; Flaherty, D. W. Catalytic Thiophene Oxidation by Groups 4 and 5 Framework-Substituted Zeolites with Hydrogen Peroxide: Mechanistic and Spectroscopic Evidence for the Effects of Metal Lewis Acidity and Solvent Lewis Basicity. *J. Catal.* **2018**, *364*, 415−425.
(56) Bonino, F.; Damin, A.; Ricchiardi, G.; Ricci, M.; Spanó, G.; D'Aloisio, R.; Zecchina, A.; Lamberti, C.; Prestipino, C.; Bordiga, S. Ti-Peroxo Species in the Ts-1/H2O2/H2O System. *J. Phys. Chem. B* **2004**, *108*, 3573−3583.
(57) Brutchey, R. L.; Ruddy, D. A.; Andersen, L. K.; Tilley, T. D. Influence of Surface Modification of Ti-SBA15 Catalysts on the Epoxidation Mechanism for Cyclohexene with Aqueous Hydrogen Peroxide. *Langmuir* **2005**, *21*, 9576−9583.
(58) Ruddy, D. A.; Brutchey, R. L.; Tilley, T. D. The Influence of Surface Modification on the Epoxidation Selectivity and Mechanism of TiSBA15 and TaSBA15 Catalysts with Aqueous Hydrogen Peroxide. *Top. Catal.* **2008**, *48*, 99−106.
(59) Yoon, C. W.; Hirsekorn, K. F.; Neidig, M. L.; Yang, X.; Tilley, T. D. Mechanism of the Decomposition of Aqueous Hydrogen Peroxide over Heterogeneous TiSBA15 and TS-1 Selective Oxidation Catalysts: Insights from Spectroscopic and Density Functional Theory Studies. *ACS Catal.* **2011**, *1*, 1665−1678.
(60) The entropies of H_2O_2 adsorption-and-activation were not measured because the decomposition of H_2O_2 occurred at high molar ratios of H_2O_2:Ti atoms, rather than only adsorption.
(61) Sever, R. R.; Root, T. W. DFT Study of Solvent Coordination Effects on Titanium-Based Epoxidation Catalysts. Part Two: Reactivity of Titanium Hydroperoxo Complexes in Ethylene Epoxidation. *J. Phys. Chem. B* **2003**, *107*, 4090−4099.
(62) Panyaburapa, W.; Nanok, T.; Limtrakul, J. L. Epoxidation Reaction of Unsaturated Hydrocarbons with H_2O_2 over Defect TS-1 Investigated by ONIOM Method: Formation of Active Sites and Reaction Mechanisms. *J. Phys. Chem. C* **2007**, *111*, 3433−3441.
(63) Ahunbay, M. G. Monte Carlo simulation of water adsorption in hydrophobic MFI zeolites with hydrophilic sites. *Langmuir* **2011**, *27*, 4986−4993.
(64) Verma, P. K.; Kundu, A.; Puretz, M. S.; Dhoonmoon, C.; Chegwidden, O. S.; Londergan, C. H.; Cho, M. The Bend+Libration Combination Band Is an Intrinsic, Collective, and Strongly Solute-Dependent Reporter on the Hydrogen Bonding Network of Liquid Water. *J. Phys. Chem. B* **2018**, *122*, 2587−2599.
(65) 1,2,-Epoxyoctane. https://www.chemicalbook.com/SpectrumEN_2984-50-1_IR2.htm (accessed March 4th, 2019).
(66) Silverstein, K. A. T.; Haymet, A. D. J.; Dill, K. A. The Strength of Hydrogen Bonds in Liquid Water and Around Nonpolar Solutes. *J. Am. Chem. Soc.* **2000**, *122*, 8037−8041.
(67) Walrafen, G. E.; Chu, Y. C. Shear Viscosity, Heat Capacity, and Fluctuations of Liquid Water, All at Constant Molal Volume. *J. Phys. Chem.* **1991**, *95*, 8909−8921.
(68) Striolo, A. Chapter 10 Nano-confined water. *Theor. Comput. Chem.* **2007**, *18*, 245−274.
(69) Munoz-Santiburcio, D.; Marx, D. Chemistry in nanoconfined water. *Chem. Sci.* **2017**, *8*, 3444−3452.
(70) Chandler, D. Interfaces and the driving force of hydrophobic assembly. *Nature* **2005**, *437*, 640−647.
(71) Anslyn, E. V.; Dougherty, D. A. *Modern Physical Organic Chemistry*; University Science: 2005.
(72) Williams, A. *Free Energy Relationships in Organic and Bio-Organic Chemistry*; Royal Society of Chemistry: Cambridge, U.K., 2003.

DOI: 10.1021/acscatal.9b03323
ACS Catal. 2019, 9, 10951−10962